In-Situ Interfacial Polymerization: A Technique for Rapid Formation of Highly Loaded Carbon Nanotube-Polymer Composites.

*Cécile A. C. Chazot, Carolyn K. Jons, and A. John Hart**

C. A. C, Chazot, C. K. Jons
Department of Materials Science and Engineering
Massachusetts Institute of Technology
Cambridge, MA 02139, USA

Prof. A. J. Hart
Department of Mechanical Engineering
Massachusetts Institute of Technology
Cambridge, MA 02139, USA
E-mail: ajhart@mit.edu

Keywords: carbon nanotubes, polymerization, interface, composites, mechanics

Abstract

Composites of polymers and organized carbon nanotube (CNT) networks have been proposed as next-generation lightweight structural materials, yet polymer infiltration of CNT networks often results in stress-concentrating heterogeneities, due to local CNT aggregation or incomplete infiltration. Herein, it is demonstrated that dense CNT-polymer composites with tailored polymer distribution can be obtained by interfacial polymerization (IP), performed *in-situ* within CNT networks. Three regimes of

This is the author manuscript accepted for publication and has undergone full peer review but has not been through the copyediting, typesetting, pagination and proofreading process, which may lead to differences between this version and the Version of Record. Please cite this article as doi: 10.1002/adfm.202005499.

the *in-situ* interfacial polymerization (ISIP) process are identified: a reaction-limited regime where the polymer forms beads on the CNTs; a uniformly-filled regime with polymer throughout the CNT network; and a transport-limited regime where polymer only forms near the outer surfaces. Uniform polyamide-CNT composite sheets obtained by this method have a Young's modulus of 31 GPa and a tensile strength of 776 MPa, which is a two-fold increase compared to the pristine CNT sheets. Overall, premature failure of the composites is attributed to large voids in the pristine CNT sheets, suggesting that further improved mechanical properties can be achieved with a more homogeneous CNT network. Nevertheless, the rapid rate and overall controllability of ISIP suggest its viability for formation of polymers within CNT networks via roll-to-roll methods.

1. Introduction

CNT-polymer composites are promising materials for high-performance structural applications, as they combine the high strength and low density of CNTs with the ductility and versatility of polymers. Early research on CNT-polymer composites focused primarily on bulk dispersion methods of CNTs in a polymer matrix, which only allows for the addition of low CNT contents (on the order of a few wt.%), and therefore only gives slight enhancements in mechanical properties relative to the polymer.[1] Yet, advances in floating catalyst based chemical vapor deposition (FC-CVD) of CNTs,[2] have enabled the formation of CNT assemblies such as sheets[3] or fibers[4] in a continuous fashion. As a result, there has been a strong interest in creating highly loaded CNT-polymer composites using CNT yarns or sheets, particularly using manufacturing techniques well-known in the fiber composites industry such as resin impregnation and curing.

High CNT content composites are most often obtained by infiltration of CNT networks with a polymer solution or a polymer melt.[5] However, direct polymer infiltration of CNT networks results in composites with heterogeneous morphologies and poor mechanical properties, due to stress concentrations at voids within the composite. These voids generally arise from CNT aggregation, resulting polymer-rich regions, as well as from the differential mobility of polymer chains with different lengths.[5] Additionally, many polymers used for structural and aerospace applications, such as aramids, feature low solubility in most common solvents and have high melting points, making them incompatible with direct infiltration techniques. Other methods, in which solutions of nanofibers such as aramids combined with CNTs, are cast to form a composite film, have been explored.[6] However, the composites obtained by this technique feature low CNT content (1.5-7.5 wt.%), due to the limited ability to disperse the CNTs and nanofibers in solution.

One approach to overcome infiltration limits of polymers in dense CNT networks is to first infiltrate a monomer, and then polymerize the monomer it *in-situ* by free-radical bulk polymerization[7–9] or electropolymerization.[10–12] While the morphology of composites obtained using this method is more uniform than in the case of polymer infiltration, the mechanical properties of the final composites are usually inferior due to use of polymers with mechanical properties unsuitable for high modulus and high strength applications, such as polystyrene, poly(methyl methacrylate) or polyaniline.[9,13] Moreover, chain-growth reactions, particularly bulk polymerization, are usually slow with reaction rates on the order of 10^{-5} mol $L^{-1}.s^{-1}$ and reaction times on the order of hours or days.[14] Therefore, toward manufacturing of structural CNT-polymer composites, it is highly desirable to have a means of forming high-performance polymers rapidly within CNT networks.

Interfacial polymerization (IP) is a type of polycondensation reaction where a polymer is formed at the interface between two liquids, each containing one or more reactive monomers.[15] The most common embodiment of IP consists of the formation of polyamides at the interface between an aqueous solution containing a diamine monomer, and a water-immiscible organic solvent containing an acid chloride (or acyl chloride) monomer. IP typically uses highly reactive monomers; the reaction rate is ~10^4-10^5 mol L^{-1} s^{-1}, and films form in seconds.[15] IP is used in fiber spinning,[16] coating of fabrics in the textile industry,[17] and the preparation of thin film composite membranes for water desalination.[18] By choice of the monomers and their functionality, IP can result in a broad range of polymer types (e.g. polyamides, polyimides, polyureas) and morphology (e.g. linear chains or crosslinked network). IP has also been used to form composites of CNTs with aliphatic polymers, but this was done by dispersing CNTs in the organic solvent which limited the CNT content of the final composite to ~1 wt.%.[19–21]

Herein, we present a versatile and scalable approach to manufacture dense CNT-polyamide composites, via interfacial polymerization within CNT sheets. The choice of the organic solvent, and the monomer concentrations, enable control of the polymer loading and distribution in the CNT sheet. Using IP of poly(m-phenylene isophthtalamide) (PMPI) as a model system, we combined elemental analysis, electron microscopy, thermal analysis, uniaxial tensile testing and fractography to identify the influence of monomer concentration and solvent type on the PMPI properties and its spatial distribution within the CNT network. Building on these observations and the kinetics theory of interfacial polycondensation, we provide insight on the design of the IP process in order to obtain tunable morphologies, ranging from discontinuous polymer-coated CNTs to monolithic dense CNT-polymer composites.

2. Results

To explore the use of ISIP for the formation of dense CNT-polymer composites, we used the polycondensation reaction (Figure 1a) of a diamine monomer (dissolved in water) with an acid chloride monomer (dissolved in a water-immiscible organic solvent). We chose R and R' to be meta-phenyl groups because these groups are known to form π-π interactions with CNTs, which are stronger than Van der Waals forces.[5] The process is performed as follows (Figure 1b): a CNT sheet is first immersed in an aqueous solution containing m-phenylene diamine. After a set time, the sheet is removed from the solution, excess liquid is flung off, and then the sheet (still imbibed with the aqueous solution) is immersed in an organic solvent (chloroform or cyclohexanone) with dissolved isophthaloyl chloride. The IP reaction occurs in the organic solvent at the liquid-liquid interface, and polymer chains precipitate when reaching a critical length due to their low solubility in the organic solvent. A custom-built reactor featuring a rotating carousel allowed the simultaneous immersion of up to six CNT sheets in the reaction medium (Figure 1c). After removal, rinsing, and drying, PMPI is found to be distributed in the CNT network (Figure 1d,e). The DC electrical conductivity of the CNT-PMPI composites increases slightly compared to the neat CNT sheets (Figure S1a, b), indicating that ISIP does not reduce the number of CNT-CNT contact points within the sheet, which would result in a decrease of the conductivity. We attribute the increase in DC conductivity upon formation of PMPI to the interplay of multiple factors. Polymer appears to precipitate preferentially around the contact points between CNTs (Figure S1c), and we hypothesize that polymerization around CNTs at contact points could result in a decrease in the contact resistance and therefore an increase in the overall conductivity of the composite. Subsequently, with increasing monomer concentration, more PMPI is produced at these locations and overall, resulting in a further conductivity increase of the composite. Additionally, capillary forces could also cause slight densification of the CNT network upon infiltration of the solvent. However, further investigation is necessary to identify the exact influence of the identified phenomena on the electrical properties of the CNT-polymer composites.

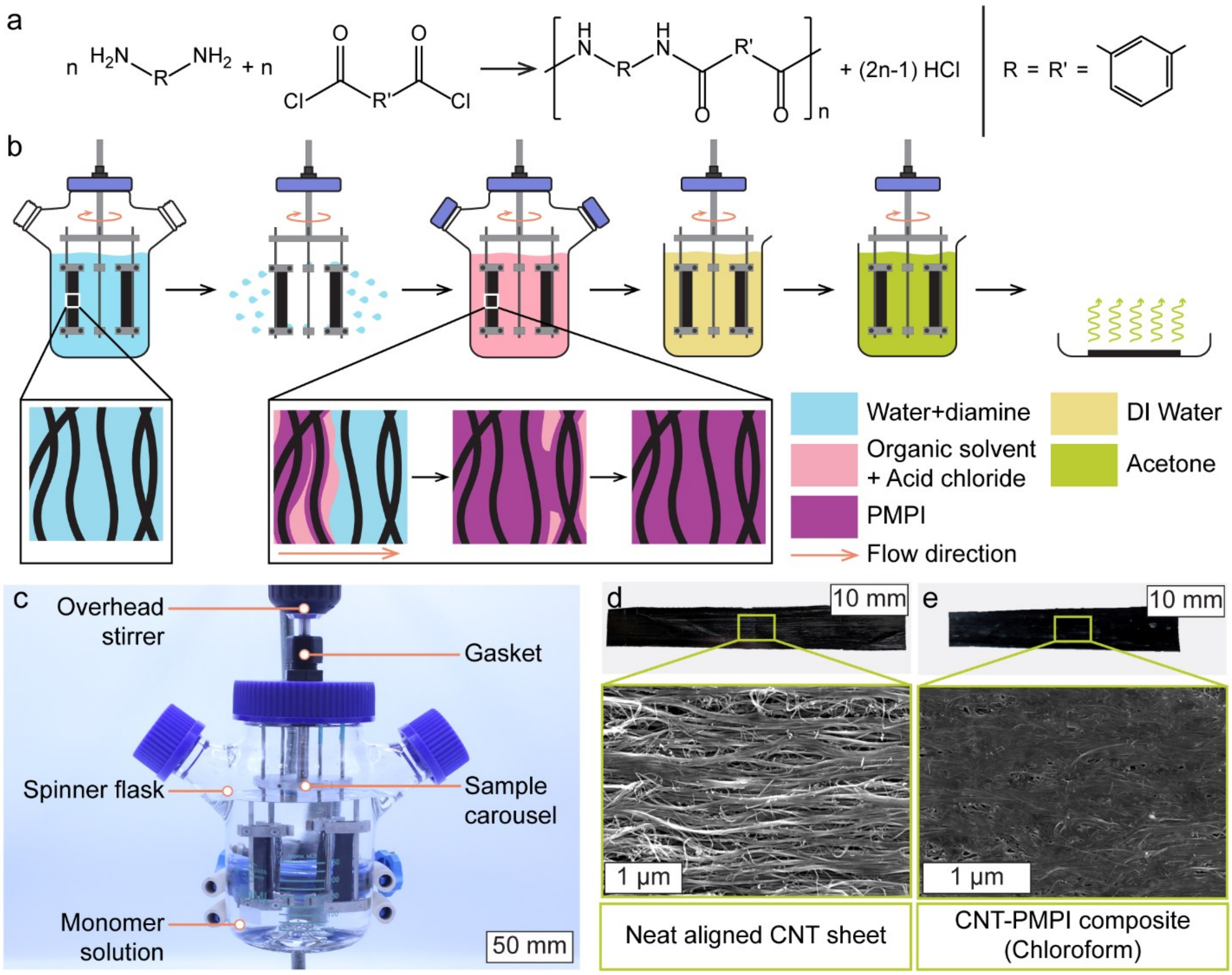

Figure 1. Polymer formation by interfacial polymerization in a CNT network. (a) Interfacial polycondensation reaction resulting in the formation of a polyamide. Herein, R and R' are both meta phenyl rings. (b) Schematic depicting the formation of a polyamide in a CNT network by interfacial polymerization. The nanoporous network is first immersed in an aqueous solution containing the diamine monomer. It is then transferred to an organic solvent containing the acid chloride monomer. The organic phase displaces the water phase and the acid chloride reacts immediately with the diamine, forming polyamide and a byproduct (hydrochloric acid). Rinsing steps remove impurities (unreacted monomer and byproduct) to result in a dense CNT-polymer composite. (c)

Front-view of the ISIP reactor. (d,e) Optical and SEM images show the top view of CNT sheets (d) before, and (e) after ISIP using chloroform as the organic solvent.

2.1. Key considerations for ISIP

To guide understanding of the relationship between synthesis conditions and final morphology, we first present an interpretation of the mechanism of ISIP in CNT sheets. After the first immersion step, the CNT network retains the aqueous solution of m-phenylene diamine within its porosity. Plunging the water-saturated network in the organic phase results in interplay between the capillary-driven flow through which the isophthaloyl chloride solution displaces the aqueous phase, and the polymer formation and precipitation near the moving liquid-liquid interface (Figure 1b). Additionally, IP occurs on the organic side of the interface; m-phenylene diamine molecules diffuse from the aqueous phase into the organic solvent before reacting with the isophthaloyl chloride molecules. As a result, the ISIP process involves two main governing rates (in mol L^{-1} s^{-1}):

- $R_{trans} = R_{capi} + R_{diff}$ which encompasses the contribution of the capillary-driven transport (R_{capi}) due to the motion of the liquid-liquid interface—influenced by relative surface energies of the two liquids and the CNTs—and the diffusive term (R_{diff}) which represents the diffusion of the diamine monomer through the liquid-liquid interface, from the aqueous to the organic solution.
- R_{rxn} which is the rate of the polycondensation reaction between m-phenylene diamine and isophthaloyl chloride in the organic phase (Figure 1a).

The relative magnitudes of these two rates define the final morphology of the composite (Figure 2a). On the one hand, to obtain uniform polymer loading, the rate of polymerization R_{rxn} must not be so rapid such that the voids within the CNT network become obstructed with solid polymer before the organic phase has fully imbibed the network. In the case where $R_{trans} < R_{rxn}$, we say the process is "transport-limited". On the other hand, if $R_{trans} > R_{rxn}$, the process is said to be "reaction-limited" and the reaction may be so slow that polymer only partially fills the interior of the CNT sheets after immersion times of ~minutes. In the case where the two rates are comparable ($R_{trans} \sim R_{rxn}$), a uniform, dense composite can be obtained, with the polymer completely filling the void space within the CNT network.

The imbibition kinetics through the network (captured by rate R_{capi}) depend on the characteristics of the CNT network, including the CNT diameter distribution, packing density, and alignment. In this study, we focused on aligned sheets of multi-walled CNTs (MWCNTs) obtained by a floating catalyst CVD method[22] (Figure 1c). The generally hydrophobic nature of MWCNTs[23] and their resulting stronger affinity with the organic solution than with the aqueous solution informed the sequential order of the liquid phases in which the CNT sheets were immersed.

Additionally, R_{diff} depends on the miscibility of the organic solvent with water. A solvent featuring higher water miscibility results in higher values of R_{diff}. From this perspective, to evaluate the influence of the solvent water miscibility on the final composite morphology and properties, composites made using chloroform (miscibility of 8.1g L^{-1} in water at room temperature)[24] and cyclohexanone (miscibility of 87g L^{-1} in water at room temperature)[25] were compared.

For a given solvent, the rate-limiting step and therefore the final morphology can be adjusted by tuning the monomer concentration (Figure 2b).[26] Assuming that the polymer precipitates immediately after the polymerization proceeds, we can consider that all the rates are equal to their initial value at t=0: $R^o_{trans} = R^o_{capi} + R^o_{diff}$ and R^o_{rxn}. We consider that both R^o_{diff} and R^o_{rxn} are dependent on the initial monomer concentrations of m-phenylene diamine $[NH_2]_o$ and isophthaloyl chloride $[COCl]_o$, while R^o_{capi} is a constant for a given solvent as it only depends on the surface energy of the organic phase. Additionally, we consider that both monomers are present in a 1:1 molar ratio so that $[NH_2]_o = [COCl]_o = [M]_o$ as these conditions lead to the highest molecular weight polymer, according to reaction stoichiometry and experimental observations.[15] From there, we can write the concentration dependence of the diffusivity rate as

$$R^o_{diff} = k_{diff} \frac{\Delta[M]_o}{d}$$

where k_{diff} is the rate constant characteristic of the diffusion of diamine from the aqueous solution to the organic solution, d is the diffusion distance at the liquid-liquid interface, and $\frac{\Delta[M]_o}{d}$ is the gradient of monomer concentration between the aqueous phase and the organic phase. Considering there is no diamine in the organic solution initially, and that d is a constant, we write:

$$R^o_{diff} = k_{diff} \frac{[M]_o}{d} = k_{diff,eff}\,[M]_o$$

In this case, $k_{diff,eff}$ is determined by the solvent type.

Next, the dependence of polymerization reaction rate on monomer concentration $[M]_o$ can be written according to the kinetics established for the polymerization reaction. We consider that polymer forms through the self-catalyzed reaction mechanism[26] of addition-elimination (Figure S2). First, a nucleophilic attack occurs on the positively-charged carbon atom in the acyl chloride functional group by the lone pair on the nitrogen atom in the amine functionality. Then, the carbon-oxygen double bond reforms and a chloride ion is pushed off and recombines with the hydrogen ion from the nitrogen to form HCl. From there, we can write:[26]

$$R_{rxn}^{o} = k_{rxn}[NH_2]_o[COCl]_o[COCl]_o = k_{rxn}[M]_o^3$$

Here, k_{rxn} is the rate constant of reaction and is assumed to be independent of solvent type.

Qualitatively, in Figure 2b we show how R_{rxn}^{o} and R_{trans}^{o} depend on $[M]_o$. The concentration range $d[M]_o^{crit}$ near $[M]_o^{crit}$, within which both rates are comparable and uniform polymer composites can be obtained, depends on the angle θ between the curve R_{rxn}^{o} and the R_{trans}^{o} line at $[M]_o^{crit}$. For a uniform loading of polymer to be created, the difference between R_{rxn}^{o} and R_{trans}^{o} must be less than some finite value dR_{crit}. The range of concentrations amenable to this regime decreases as θ increases. Qualitatively, for large values of θ, the parameter range giving uniform polymer loading may be difficult to assess expeimentally, as a small change in $[M]_o$ immediately results in a direct transition from the transport-limited regime to the reaction-limited regime. As θ is directly related to the slope and intercept of R_{trans}^{o}, it is determined by solvent type.

The present study focuses on varying monomer concentration to identify the different kinetic regimes for the two chosen organic solvents, specifically cyclohexanone and chloroform, and relates the rate-limiting step to the final morphology and mechanical properties of the obtained CNT-PMPI composites. In what follows, we first combine electron microscopy, elemental analysis and thermogravimetric analysis to identify the different kinetic regimes associated with the ISIP conditions, as well as the nature of the polymer formed and the CNT-PMPI interaction. Second, we focus on assessing the multiscale morphology of the composites and its influence of the final mechanical properties of the CNT-PMPI composites obtained in the defined kinetics regimes.

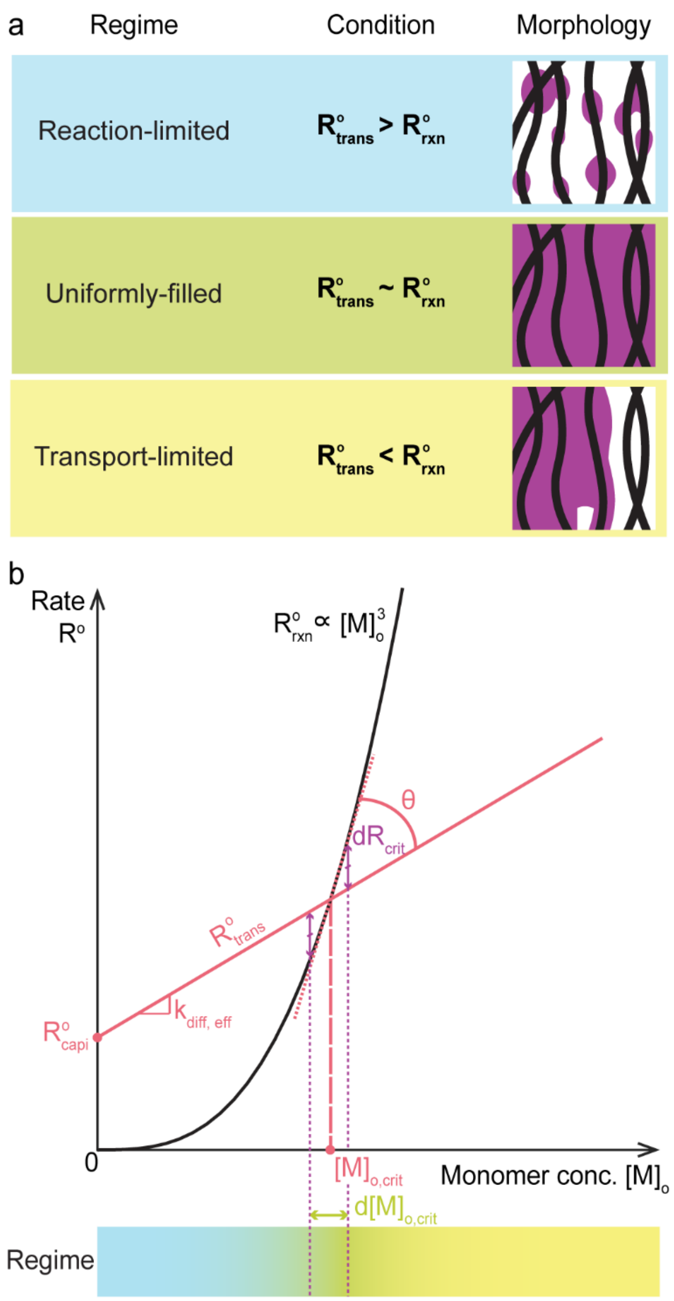

Figure 2. Relative rate dependence and resulting final composite morphology. (a) Definition of the different kinetics regimes based on the relative magnitudes of the transport rate and the reaction rate, as well as the expected resulting morphology. (b) Qualitative representation of the dependence of the different rates involved in ISIP on monomer concentration.

2.2. Assessment of polymer content variation and rate-limiting step

Guided by kinetics theory, we now show how to produce CNT-polymer composites with tailored polymer morphology by ISIP. This is accomplished by adjusting the relative magnitudes of the transport and reaction rates by varying the solvent type and $[M]_o$.

Energy Dispersive X-Ray Spectroscopy (EDS) was used to assess polymer content variation throughout the thickness of the CNT composites (Figure 3), as well as the presence of potential byproducts or residual solvent. Neat CNT sheets show nitrogen (N) and a chlorine (Cl) content on the order of 0.1 ±0.01at.% (Figure 3a), allowing us to use the N signal as a measure of the polymer content versus depth. Additionally, the Cl signal increases between the neat CNT sheets and the CNT-PMPI composites (Figure 3b-d), particularly in the case where chloroform is used as the solvent. This increase is attributed to the amount of residual by-product (HCl) and chloroform trapped in the polymer, which could not be washed off nor evaporated due to the dense and tortuous CNT-PMPI composite structure.

CNT-PMPI composites obtained with cyclohexanone and chloroform at equivalent monomer concentration (0.15 mol L^{-1}) exhibit very different spatial distributions of the polymer content throughout the thickness of the CNT sheet. The CNT-PMPI composite formed with cyclohexanone shows a constant polymer loading throughout the thickness (Figure 3b), indicating that a $[M]_o$ of

0.15 mol L^{-1} resulted in $R_{trans}^{cyclo} \geq R_{rxn}^{cyclo}$, i.e., the reaction-limited or uniformly-filled regime as defined in Figure 2a. The uniformity of polymer distribution is further confirmed by 2D EDS mapping (Figure S3 and Table S1). Conversely, IP using chloroform produces a gradient of polymer content, decreasing toward the center of the CNT sheet. (Figure 3c). This suggests that the same $[M]_o$ resulted in $R_{trans}^{chloro} < R_{rxn}^{chloro}$ i.e., the transport-limited regime.

This observation is explained by the dependence of solvent transport rate on its miscibility with water. Cyclohexanone features a water miscibility 20 times greater than chloroform, resulting in faster diffusion of m-phenylene diamine through the interface. From this perspective, the slope of R_{trans}^{o} with $[M]_o$ is greater in the case of cyclohexanone (Figure 2b) and the uniformly-filled regime occurs at a higher $[M]_o^{crit}$. However, for $[M]_o$=0.17 mol L^{-1} in cyclohexanone, non-uniform polymer distribution is obtained (Figure 3d) indicating that the increase in monomer concentration results in $R_{trans}^{cyclo} < R_{rxn}^{cyclo}$, i.e. the transport-limited regime is reached. Transmission Electron Microscopy (TEM) images (Figure 4) of a thin (~60 nm) cross-section of a CNT-PMPI composite obtained in cyclohexanone at $[M]_o$=0.15 mol L^{-1}, also suggest uniform polymer loading throughout the thickness of the sheet with no apparent residual voids (Figure 4a). Nevertheless, the large amount of polymer and the thickness of the cross-section in those conditions does not enable high-resolution imaging and assessment of the crystallinity of the PMPI formed by ISIP. From this perspective, cryo-FIB was performed to isolate lamellae from the core of CNT-PMPI composites obtained in the transport-limited regime. Those lamellae exhibit lower polymer content and enable high-resolution TEM images of isolated CNTs and PMPI (Figure 4b), showing that PMPI synthesized by ISIP forms an amorphous solid coating on the CNTs, which prevents the observation of the crystalline planes of the CNT walls by TEM (Figure 4c).

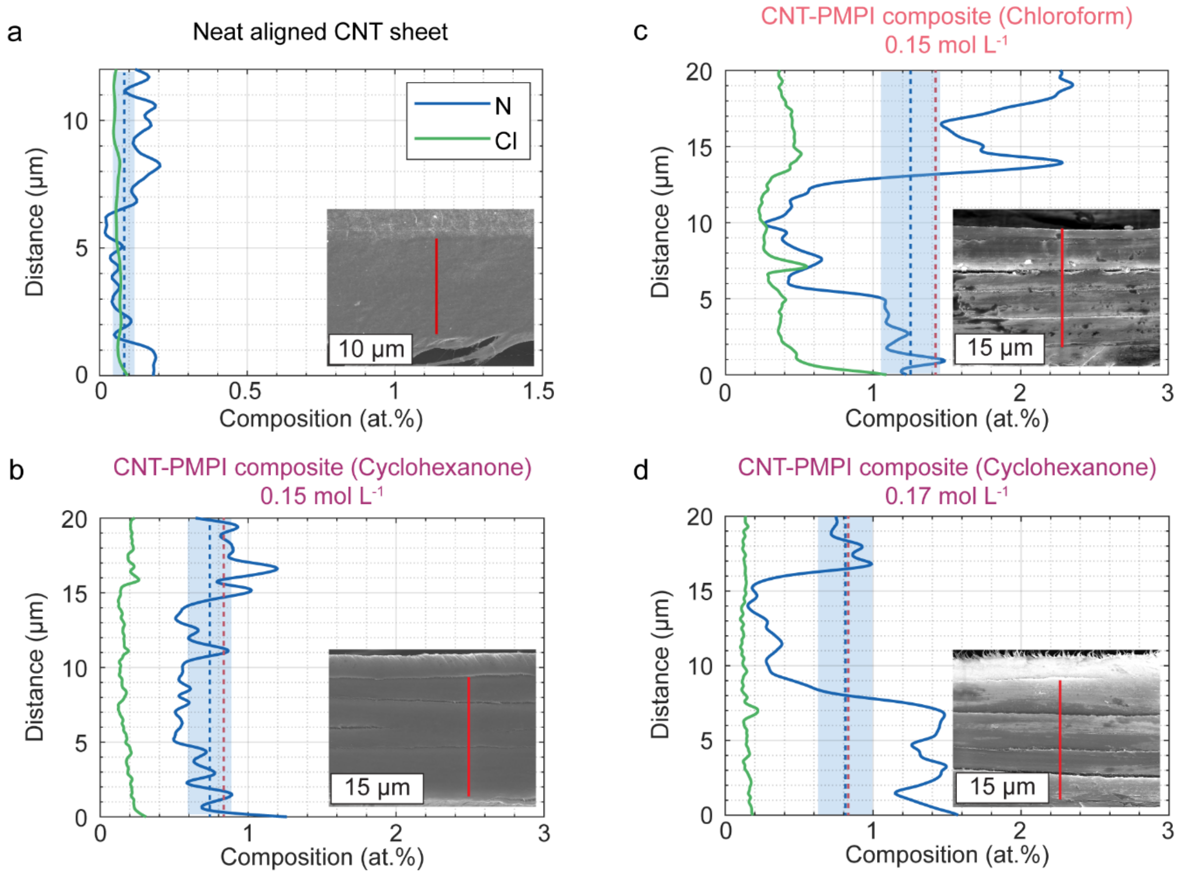

Figure 3. EDS line profile through the cross-section of (a) the bare CNT sheet, and (b-d) composite sheets obtained using $[M]_o$ = 0.15 mol L^{-1} in (b) cyclohexanone and (c) chloroform as the organic phase, and (d) $[M]_o$ = 0.17 mol L^{-1} in cyclohexanone. Nitrogen is one of the main elements that is present in the polymer chain, but not in the CNTs. Chlorine is the result of residual hydrochloric acid or chlorinated solvent in the system. The blue dashed line indicates the average at.% of nitrogen while the shaded area is the error of the EDS measurement. The red dashed line is the expected at.% N calculated from TGA measurements. Inset images show scanning electron micrographs of the cross-sections of the relevant samples and the red lines show where the EDS scans were performed.

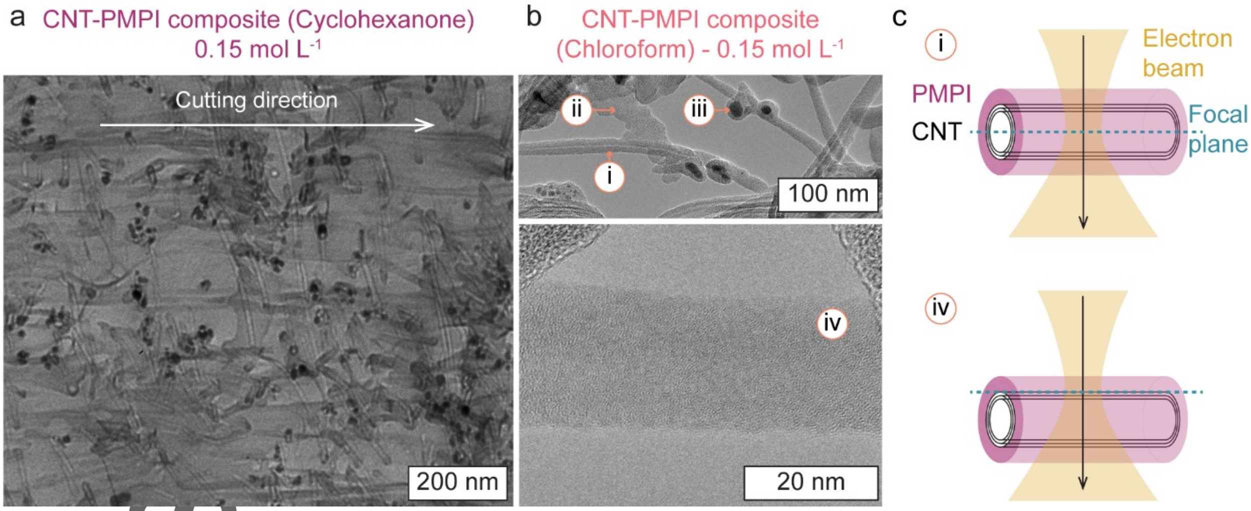

Figure 4. TEM images of CNT-PMPI composites. (a) Microtome section of a CNT-PMPI composite showing uniform PMPI loading. Compression and shear during the cutting process result in some CNTs aligning along the cutting direction. (b) TEM view of a CNT-PMPI lamella obtained by Cryo-Focused Ion Beam (FIB) from a composite sample formed in chloroform. (i) A sheath of PMPI formed around a single CNT, (ii) neat PMPI bridging between CNTs, and (iii) a residual iron catalyst particle embedded in PMPI. (iv) Higher magnification of the PMPI-wrapped CNT shows the pattern typical for amorphous material. (c) Schematics explaining the different appearance in TEM images of PMPI-wrapped CNTs, depending on the focus of the electron beam. Regardless of the beam focus location, the crystalline planes of the CNT walls cannot be resolved due to the amorphous nature of the PMPI coating. When the electron beam is focused on the center of the CNT, a higher brightness line can be seen as the hollow center of the CNT as seen in (i). When the electron beam is focused on the surface of the CNT, the amorphous texture of the polymer dominates, and the CNT wall crystalline planes cannot be resolved, as seen in (iv).

2.3. Thermal stability of *in-situ* polymerized polyamide and the effect of CNTs

Thermogravimetric analysis was used to assess the thermal stability of PMPI synthesized by ISIP, as well as the polymer content in the final CNT-PMPI composite (Figure 5). PMPI, as well as the CNT-PMPI composites, show a significant mass loss beginning at around 400°C, corresponding to the decomposition of PMPI (Figure 5a). Note that in its neat form, the decomposition profile of PMPI is independent of solvent type and monomer concentration used in the IP process.

The relationship between polymer content and $[M]_o$is strongly influenced by the organic solvent used for ISIP (Figure 5b). For cyclohexanone, the polymer content increases with $[M]_o < 0.15$ mol L^{-1}, then remains constant at higher concentrations. In the case of chloroform, the polymer content increases monotonically with $[M]_o$ (from 0.075 to 0.28 mol L^{-1}). By EDS, we find that CNT-PMPI composites obtained in chloroform solutions with $[M]_o \geq 0.1$ mol L^{-1} feature non-uniform polymer loading, indicating the transport-limited regime at these concentrations. Similarly, we find that CNT-PMPI composites obtained in cyclohexanone solution with $[M]_o \geq 0.17$ mol L^{-1} also fall within the transport-limited regime of the ISIP process.

Compared to neat PMPI synthesized by IP in absence of CNTs, CNT-PMPI composites show a dependence of the onset temperature of thermal degradation T_{onset} with monomer concentration and solvent type (Figure 5c). In the reaction-limited regime (cyclohexanone with $[M]_o < 0.15$ mol L^{-1}), T_{onset} increases with $[M]_o$ and is greater than T_{onset} of neat PMPI. The increase in T_{onset} can be influenced by both the polymer loading, as well as variations in polymer characteristics (density, ordering) due to the presence of CNTs. First, in the reaction-limited regime, an increase of $[M]_o$ results in more PMPI being formed between the CNTs at otherwise identical IP conditions, i.e., a higher polymer content overall. We hypothesize that the greater polymer content impedes diffusion of decomposition by-products from the CNT sheet, imparting a higher measured onset temperature. As such, CNT-PMPI composites showing uniform polymer loading (cyclohexanone and $[M]_o$ of 0.15 mol L^{-1}) exhibit the highest measured T_{onset}. Chloroform does not show a uniformly-filled regime in the range of concentrations tested. Second, in the transport-limited regime, T_{onset} decreases linearly with $[M]_o$, reaching values lower than that of neat PMPI, suggesting that CNT-PMPI interaction also influences T_{onset}. In addition, the slope of the decay is independent of the solvent used for ISIP, suggesting that the CNT-PMPI interaction is governed by the chemical structure of the polymer, regardless of the solvent used for IP.

The varied evolution of polymer content with $[M]_o$ in the transport-limited regime can be understood by comparing the solubility of PMPI in the two organic solvents, and its impact of the final density of the polymer formed. In this analysis, we consider that the PMPI formed by ISIP is amorphous, as observed by Transmission Electron Microscopy (TEM) (Figure 4b) and expected from the high polydispersity which results from the IP reaction.[27] We calculate the polymer-solvent interaction parameter $\chi_{PMPI,solv}$ based on the Hildebrand solubility parameters for PMPI, cyclohexanone, and chloroform following the formalism:[14]

$$\chi_{PMPI,solv} = \frac{v(\delta_{PMPI} - \delta_{solv})^2}{RT}$$

Here v is the molar volume (m^3 mol^{-1}) of the solvent, δ_{PMPI} and δ_{solv} are the Hildebrand solubility parameters ($Pa^{1/2}$) for PMPI and the solvent respectively, $R = 8.314$ J mol^{-1} K^{-1} is the ideal gas constant, and $T = 298$ K the temperature. We consider $\delta_{PMPI} = 26.8$ $MPa^{1/2}$ as reported in the literature [28] and confirmed by Van Krevelen group contribution calculation for solubility parameters and molar volumes.[28] The values $\delta_{cyclo} = 19.6$ $MPa^{1/2}$, $v_{cyclo} = 104$ mL mol^{-1}, $\delta_{chloro} = 19.0$ $MPa^{1/2}$, and $v_{chloro} = 80.7$ mL mol^{-1} for cyclohexanone and chloroform were taken from the literature.[28]

We find that $\chi_{PMPI,chloro} = 1.98$ and $\chi_{PMPI,cyclo} = 2.18$. This is in agreement with the experimental observation that both chloroform and cyclohexanone are poor solvents for the polymer ($\chi > 0.5$), and result in precipitation of PMPI upon polymerization. Nevertheless, chloroform is a better solvent for the polymer (lower χ), suggesting that it can swell the solid PMPI forming at the surface of the CNTs to a greater extent, allowing for reactive monomer molecules to be trapped in the network (Figure 5d). We hypothesize that, with time, more polymer chains form from the trapped monomers and densify the solid PMPI coating attached to the CNTs, as this has been observed for multiple polyamide systems formed by traditional IP at a liquid-liquid interface.[29] Cyclohexanone does not result in as much swelling of the polymer, and the mass density of the polymer stays constant, resulting in a stagnation of the polymer content with $[M]_o$.

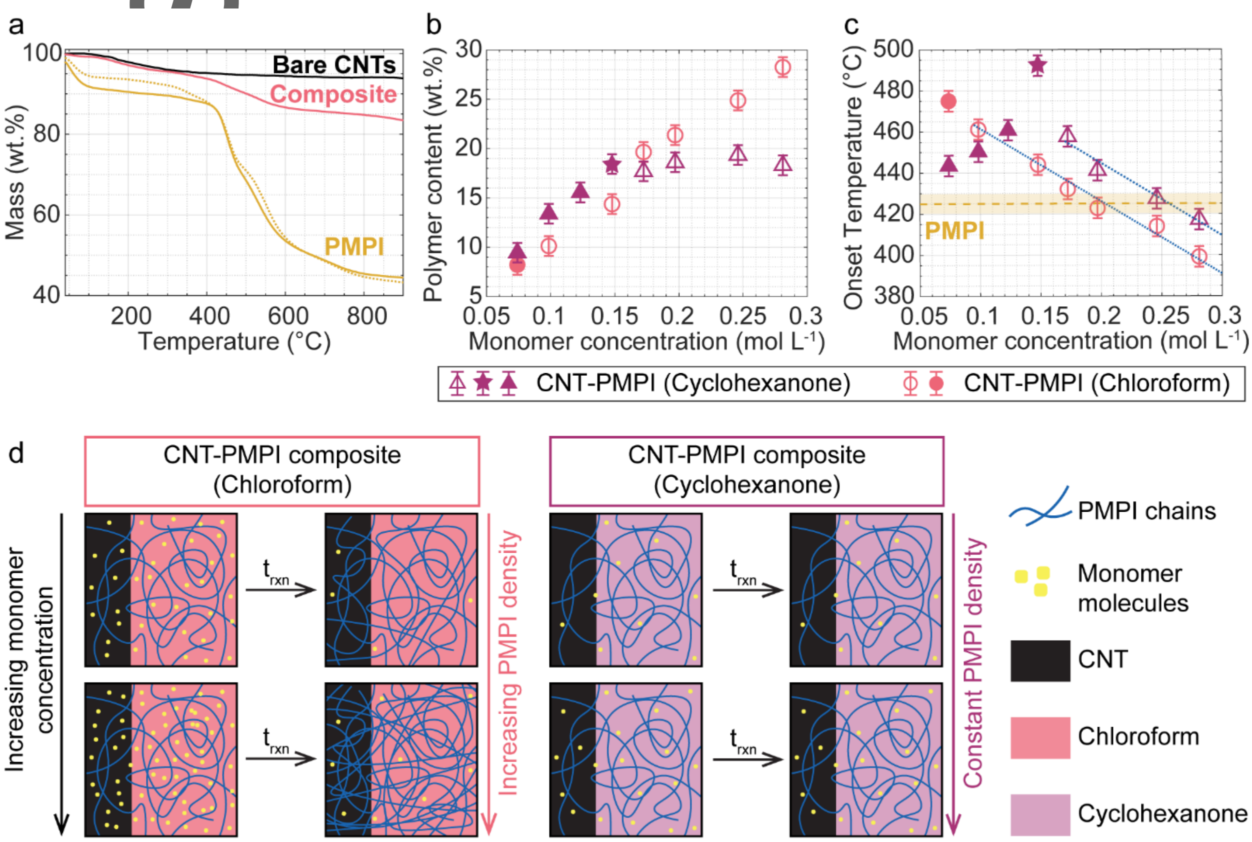

Figure 5. Thermogravimetric analysis (TGA) of the CNT-PMPI composites. (a) Representative TGA decomposition profiles obtained for the bare CNT structure, the pure polymer, and the composite. The solid and dashed yellow lines correspond to PMPI synthesized by IP in the absence of CNTs in chloroform and cyclohexanone, respectively. (b) Evolution of the polymer content in the composite with monomer concentration. (c) Evolution of the decomposition temperature of the PMPI in the

composite with monomer concentration. Filled markers correspond to the reaction-limited regime, star-shaped markers to the uniformly-filled regime, and empty markers to the transport-limited regime. The error bars represent the standard deviation of values obtained from analysis of three samples in each polymerization condition. The average value of decomposition temperature (yellow dashed line) for PMPI synthesized in the absence of CNTs, and standard deviation between samples synthesized under the same conditions (yellow shaded area) are also plotted for comparison. (d) Schematics explaining the qualitative evolution of PMPI density with monomer concentration, depending on the organic solvent. t_{rxn} refers to the duration of the ISIP reaction.

2.4. Mechanical properties and fracture mechanics

Mechanical properties also guide interpretation of the CNT-PMPI composite morphology, and the role of homogeneity and polymer distribution at larger length scales. Uniaxial tensile testing was performed on CNT-PMPI composite sheets obtained by ISIP (Figure 6). The composite samples were cut into dog-bone specimens following the ISO-37 standard (Type 4 geometry) for tensile testing. Load was applied along the alignment direction of the CNTs. Representative engineering stress-strain curves for the bare aligned CNT sheet and the ISIP composites (Figure 6a) indicate a toe region followed by a linear region. The toe region is attributed to the rearrangement of the CNTs, which become more uniformly aligned along the loading direction with increasing strain. This is a characteristic behavior of CNT assemblies[30], as well as biological fiber-reinforced composites[31] and nanofiber mats.[32] The maximum stress corresponds to the initial failure point in the gauge region. Upon further loading, the specimen exhibits decreased stiffness but continues to carry load until final failure. We observed that all specimens develop multiple local failures. This is commonly observed for both CNT neat assemblies[33] and composites,[34] as well as carbon fiber composites[35,36] and is attributed to sequential failure CNT bundles and CNT-polymer interfaces, as well as redistribution of stress as loading proceeds.

CNT-PMPI composites obtained with cyclohexanone in the uniformly-filled regime exhibit significantly higher values of elastic modulus (Figure 6b) and tensile strength (Figure 6c) compared to both the neat aligned CNT sheets and the CNT-PMPI composites obtained in the reaction-limited and transport-limited regimes. The same trend is observed for specific modulus and specific strength (Figure S4). Specifically, uniformly-filled CNT-PMPI composites exhibit an elastic modulus of 31 GPa (22 N Tex^{-1}) and a tensile strength of 776 MPa (0.56 N Tex^{-1}); these values are 2.0- and 2.3-fold greater, respectively, than the values for neat aligned CNT sheets. On the other hand, for both chloroform and cyclohexanone, CNT-PMPI composites obtained in the reaction-limited and transport-limited regime show values of elastic modulus and tensile strength of 24 GPa and 600 MPa.

While the above results show significant increases in both the absolute, and density-normalized tensile properties, the modulus and strength of both the CNT networks and the composites are far below expectations for highly-ordered, dense CNT materials.[5] We attribute this difference to the presence of voids in the starting CNT sheets, as confirmed by X-ray computed tomography (CT) (Figure 6d-g). These voids result from the manufacturing technique used to form the CNT sheets. In the floating catalyst CVD method, the CNTs form an aerogel-like “sock” which collapses prior to mechanical collection from the furnace; this resulting CNT sheet is then aligned by wet-stretching[22] to form the CNT ribbons used as a starting material in this work. As the sock forms, it typically has a highly entangled web of CNTs on the outer surface, and a low-density, low-entanglement core where the carrier gas mainly flows.[37] The invariance of the modulus and strength with $[M]_o$ in the reaction-limited and transport-limited regime suggests that the flaws resulting from the CNT sheet morphology cause preferential failure via internal stress concentration within the composite.

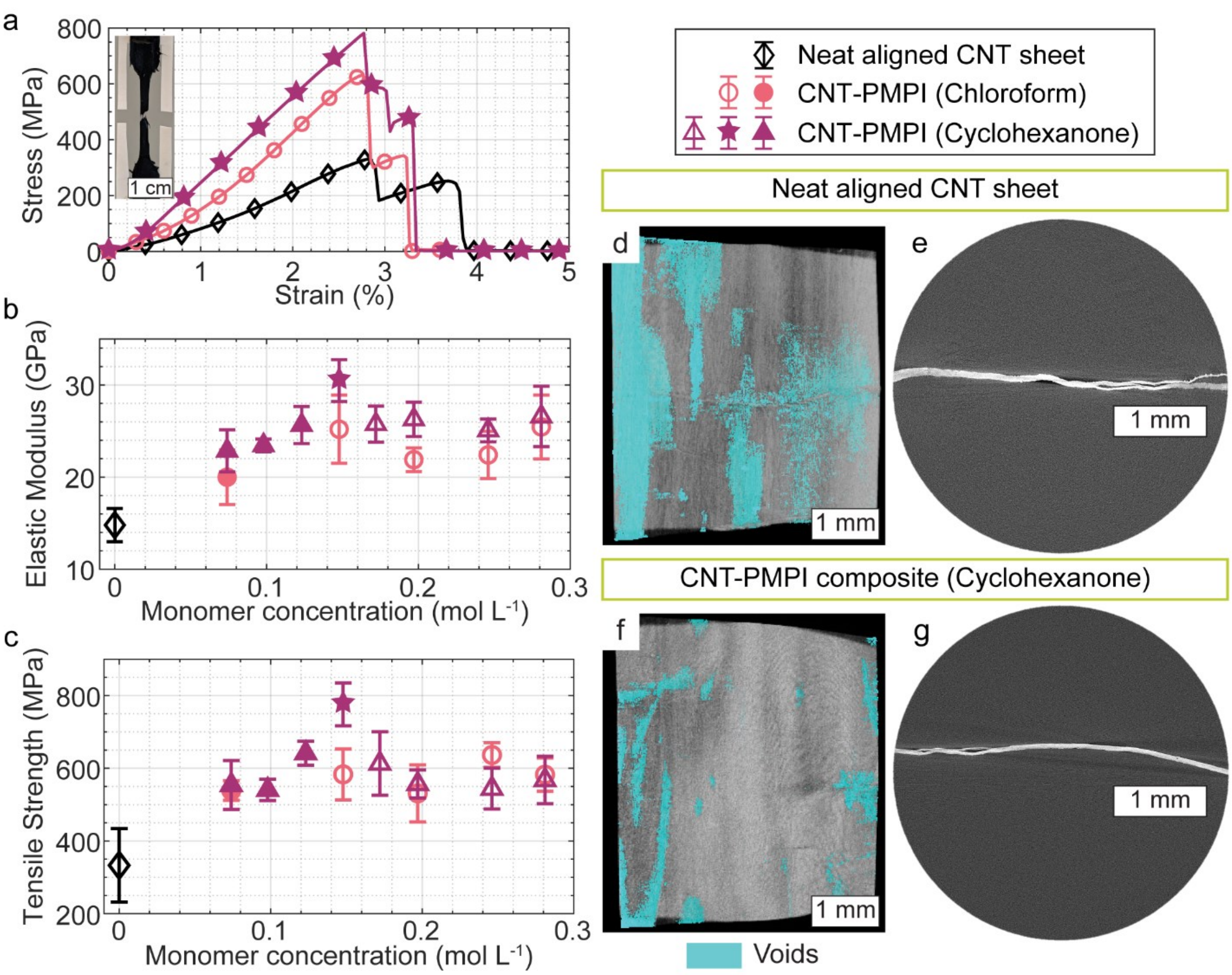

Figure 6. Mechanical properties of CNT-PMPI composite sheets. (a) Typical Stress-Strain curves for the bare CNT structure as well as the CNT-polymer composites. Inset: Dog-bone sample used for tensile testing. (b,c) Evolution of the (b) elastic modulus and (c) tensile strength with the monomer concentration. Filled markers correspond to the reaction-limited regime, star-shaped markers to the uniformly-filled regime, and empty markers to the transport-limited regime. The error bars represent the standard deviation of values obtained from analysis of between five and seven samples in each polymerization condition. (d-g) X-ray tomography reconstruction and representative slice of (d,e) a neat CNT sheet, and (f,g) a CNT-polymer composite obtained by ISIP for $[M]_o$ = 0.15 mol L^{-1} in cyclohexanone. The areas colored in blue in the reconstruction correspond to large voids (>5 µm).

Therefore, we may rely on local observations of fracture mechanics as a more useful guide to the role of polymer formed by ISIP on reinforcing the CNT network (Figure 7). SEM fractography provides visual confirmation of which IP parameters result in the reaction-limited, uniformly-filled, and transport-limited regimes (Figure 7a). At low monomer concentration ($[M]_o \leq 0.125$ mol L^{-1} for cyclohexanone and $[M]_o \leq 0.075$ mol L^{-1} for chloroform), the fracture surface of the composite reveals beads of PMPI adhered to CNTs (Figure 7b,c). At high monomer concentrations ($[M]_o \geq 0.175$ mol L^{-1} for cyclohexanone, and $[M]_o \geq 0.095$ mol L^{-1} for chloroform), the transport-limited regime results in delamination at the interface between the polymer-rich outer region and the polymer-deprived inner region (Figure 7d,e). In the uniformly-filled regime, fracture profiles show crack propagation throughout the polymer-filled region and reveal CNTs surrounded with polymer sheathings of various sizes (Figure 7f-h). The smooth cylindrical shape of the PMPI sheathing suggests that ISIP results in a strong chemical interaction between PMPI and the CNTs (Figure 7h). To the best of our knowledge, such polymer sheathing fracture morphology has only been observed in the case of poly(vinyl alcohol)[38] and polycarbonate[39] in CNT composites obtained by polymer solution infiltration. Notably, the uniformly-filled regime could only be resolved experimentally when cyclohexanone was used as the organic solvent. Indeed, we observe that incrementing $d[M]_o$ of 0.025 mol L^{-1} in chloroform results in a jump from the reaction-limited to the transport-limited regime, while in cyclohexanone the same increment corresponds to a transition from reaction-limited to the uniformly-filled regime. This suggests that the range of concentrations $d[M]_{o,crit}$ at which uniform polymer distribution can be obtained in chloroform is < 0.025 mol L^{-1}, while it is < 0.05 mol L^{-1} in the case of cyclohexanone.

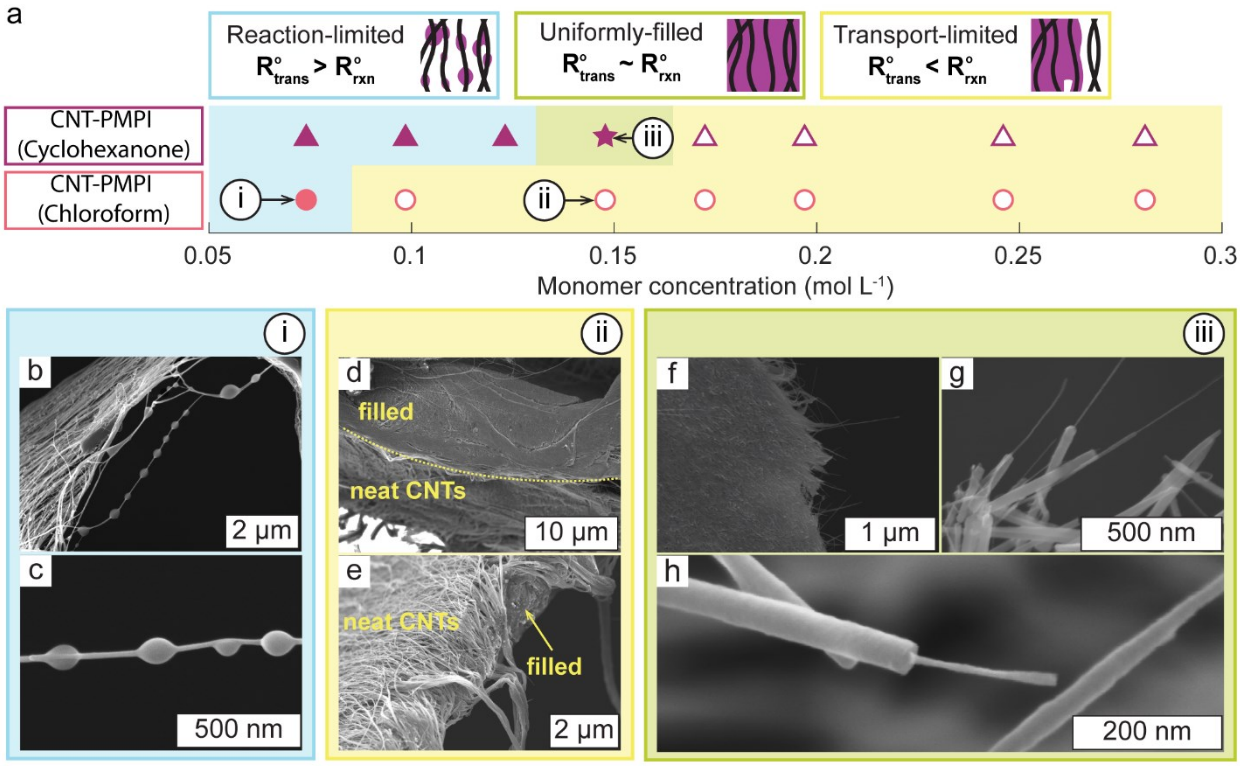

Figure 7. Fractography and nanoscale morphology. (a) Evolution of the morphology of the composites with monomer concentration and solvent type, showing three main regimes depending on the rate-limiting step, from a reaction-limited regime at low monomer concentration to a transport-limited regime at high monomer concentration. Filled markers correspond to the reaction-limited regime, star-shaped markers to the uniformly-filled regime, and empty markers to the transport-limited regime. (b-h) Corresponding fracture profiles for composites in each regime corresponding to data points (i), (ii), and (iii) as indicated in (a).

3. Discussion

ISIP enables the creation of CNT-polymer composites with tailored polymer morphology and loading. The rapid polymerization reaction could be scaled to a continuous process, as has been demonstrated in the case of thin film composite (TFC) membranes for desalination technologies, wherein thin polymer films are produced at liquid-liquid interfaces.[18,40] Additionally, the process is viable for any step-growth reactions and can be adapted to various polymer types such as polyesters,[41] polyureas,[42] or polyimides,[43] opening new range of accessible properties and potential applications. The easily CNT-aramid composites described here feature improved mechanical properties and high thermal stability, making them suitable candidates for applications such as electromagnetic shielding.

Nevertheless, the rapid polycondensation reaction rate of ISIP results in a large polydispersity index comparable to or greater than the Flory limit of 2. This high polydispersity makes the process unsuitable to produce polymers with high crystallinity. Additionally, the window of processing parameters to obtain a uniform composite may seem narrow, with only one tested concentration resulting in such morphology in the current study. However, adjusting other processing parameters such as pH of the aqueous phase, or the use of a solvent even more miscible in water such as tetrahydrofuran (THF), could broaden the concentration range $d[M]_o^{crit}$ at which the uniformly-filled morphology can be obtained. Additionally, finer control of the morphology and accurate prediction of the processing windows can be achieved through a quantitative understanding of the interplay between reaction kinetics and transport kinetics, as well as how the CNT surface and network morphology influences polymer formation and adhesion.

Importantly, ISIP features shorter processing times than direct polymer infiltration and, to our understanding, preserves the morphology of the CNT network. Improvements in the neat CNT sheet morphology, as well as local microscale mechanical characterization would enable deeper understanding of the CNT-polymer interaction and scaling of the mechanical properties to structurally relevant levels. Finally, ISIP is not limited to CNT networks and could be used to obtain composites of polymers and other porous materials such as electrospun nanofiber mats, or foams.

4. Conclusion

We show that ISIP within a nanoporous CNT assembly enables the formation of CNT-aramid composites, which cannot easily be obtained by polymer solution infiltration or melt processing due to polyamide's insolubility in most organic solvents and high melting point. We demonstrated the ability of ISIP to form CNT-polymer composites with tunable polymer loading, reaching full and uniform loading under particular conditions guided by chemical kinetics theory. Tensile strength and elastic modulus of the composites obtained by this method are superior to those of neat CNT structures and could be improved by reducing voids already present in the starting CNT material. ISIP shows potential for scale up as it not only could be applied to a wide variety of polymer systems (e.g. polyamides, polyesters, polyimides), but it also features short processing times, and the potential to be integrated in a roll-to-roll manufacturing process.

5. Experimental Section

Manufacturing and preparation of CNT sheets: CNT sheets were manufactured by Nanocomp Technologies, Inc using a floating catalyst CVD process. After synthesis, the CNT sheets are liquid-saturated and stretched by ~35%, resulting in a final CNT Herman orientation factor of 0.7.[22] The sheets also have 5-10wt.% amorphous carbon and 10-20wt.% residual catalyst. Particular attention was given to confirming the absence of carboxylic acid groups at the surface of the CNTs, as such functionalities could react with the diamine monomer molecules and result in covalent bonding of the polymer chains with the CNTs. First, elemental analysis (EDS) on neat CNT sheets reveal only a residual amount of oxygen (3.9 at.%, Table S2) which is attributed to defects at the surface of the CNTs from the CVD growth process and the presence of residual iron oxide catalyst particles. Moreover, Raman spectroscopy (Figure S5) reveals CNTs with low defect density (ID/IG ratio of 0.33) and TGA in air (Figure S6) shows no significant mass loss at 300°C, which is the expected decomposition of carboxylic groups.[44] For each ISIP experiment, pieces of the CNT sheet were mounted on the sample carousel and immersed in deionized water for 30 minutes before any immersion in monomer solutions.

Interfacial polymerization: All chemicals were used as received and did not undergo any additional purification. Isophthaloyl Chloride (≥99%) was obtained from TCI America and stored under inert atmosphere to prevent hydrolysis of the compound. M-phenylene diamine (≥99%) was purchased from Millipore Sigma and was also stored under inert atmosphere. Chloroform (containing 100-200 ppm amylenes as stabilizer, ≥99.5%), cyclohexanone (ACS reagent, ≥99.0%), water (ACS reagent), and acetone (ACS reagent, ≥99.5%) were also obtained from Millipore Sigma. Glassware was always rinsed twice with the solvent that it would contain prior to solution preparation or to the polymerization reaction. Monomer solutions were prepared by weighing the monomers and dissolving them in their respective solvents (diamine in water and acyl chloride in organic solvent) in a conical flask equipped with a magnetic stir bar. The volume of solvent was measured with a graduated cylinder. Monomer concentration in mol.L^{-1} was the same for both solutions to maintain a 1:1 molar ratio between the diamine and acid chloride. Aqueous solutions were prepared and stored in amber glassware to prevent damage of the diamine monomer which features UV sensitivity.

For ISIP a custom-made experimental setup (Figure S7) was developed in order to produce CNT-polymer composites at high throughput. A sample carousel which could hold and rotate six CNT ribbons at once was designed to rotate the samples in the sequential solutions, and machined out of chemically resistant materials (Aluminum 6061, 316 Stainless Steel, and Kalrez® rubber) (Figure S7a-c). The carousel attachment consisted of an aluminum plate with six radial slots and a set screw to fix each sample in place with regard to the disk (Figure S7a). Each CNT sample was kept under light tension by a set of custom-made clamps, mounted on a shaft and equipped with Kalrez® rubber to hold the CNT assemblies without damaging it (Figure S7b). The carousel assembly was held by a rotary shaft fixed with regard to the aluminum disk, and fits in a spinner flask featuring two 45° necks which were used for liquid addition or removal (Figure S7c). The spinner flask was sealed with a cap equipped with a gasket which prevented solvent evaporation while allowing carousel rotation inside the subsequent solvent baths at a speed of approximately 50 rpm. The experimental setup described above was used in a multiple step process to obtain CNT-PMPI composites by ISIP. The neat CNT assemblies were first immersed in an aqueous solution of m-phenylene diamine (0.075-0.28 mol.L^{-1}) for 20 minutes to ensure complete wetting of the network. The excess solution was shaken off the clamp and the outer surface of the sample by increasing the speed of the carousel to

150 rpm for 2 seconds. This allowed the aqueous phase to be retained within the network without having a film of water on the outside of the sample which could react with the organic phase and prevent the transport of the organic solvent inside the pores of the CNT assembly. The ribbons were then immersed in an organic solution of isophthaloyl chloride (1:1 molar ratio with m-phenylene diamine to preserve stoichiometry of the reaction) dissolved in chloroform or cyclohexanone. The reaction was left to proceed for 5 minutes before the resulting composite was transferred first to a DI water rinsing bath (to wash off the by-product) and second to an acetone rinsing solution (to wash off the unreacted monomers). Finally, the CNT ribbons were removed from the clamps and left to dry in air overnight.

To obtain the decomposition temperature of pure PMPI, we conducted IP at the liquid-liquid interface in a classical beaker setup, in absence of CNTs.[15] In this case, 100 mL of both solutions were used. In the case of chloroform, the chloroform solution was poured into the beaker first due to its greater density than water. In the case of cyclohexanone, the aqueous phase was denser and was at the bottom of the beaker, while the organic phase rested on top of the water phase. An aramid film formed at the interface between the two liquids immediately. As PMPI is an aromatic polyamide, the polymer chains act as rigid rods and do not feature enough entanglement to pull the film as a continuous rope from the liquid-liquid interface as it is commonly done for aliphatic polyamides. From this perspective, the beaker was equipped with a custom-made polymer film collector consisting of a 316 stainless steel mesh, supporting a circle of filter paper. Both the mesh and the filter paper had the same diameter as the beaker to maximize the amount of polymer film collected by this method. The polymer film collector was set to rest at the bottom of the beaker before the monomer solutions were poured into the reaction vessel. The mesh featured two handle accessible from the top of the beaker allowing to lift the collecting device up and collect the polymer film formed at the interface between the two liquids. After a reaction time of 5 minutes, the top phase was removed with a custom-made glass siphon and the polymer film was collected onto the filter paper by lifting up the polymer film collector. The polymer was scraped off the filter paper, rinsed twice in both water and acetone, and isolated by filtration.

Scanning Electron Microscopy and Energy Dispersive X-Ray Spectroscopy: SEM images were obtained with a Zeiss Merlin High-Resolution Scanning Electron Microscope (SEM) using the High Resolution mode, the in-lens detector, an acceleration voltage of 3kV, and a probe current of 100 pA. To obtain qualitative information about the elemental distribution throughout the thickness of the composites, Energy-Dispersive X-ray Spectroscopy (EDS) was conducted using an EDS detector and the software APEX. A line profile across the thickness of the samples, a working distance of 10 mm, a linewidth of 1 µm, an integration time of 100 ms and 16 frames were used to allow for the detection of low-atomic-number elements. In the case of EDS measurements, the acceleration voltage was increased to 10kV and the probe current to 500 pA. Considering the challenges associated with measuring small atomic number elements by EDS, we compared the average nitrogen content to the nitrogen at.% calculated from TGA measurements of the polymer content. In all cases, the average at.% nitrogen measured by EDS was within the error bars of the expected value obtained from thermal analysis, confirming that the signal actually emerged from PMPI (Figure 3b, c).

Transmission electron microscopy and associated sample preparation: Thin lamellae for TEM images were prepared by two methods. A first set of lamellae was prepared by Cryo-FIB on a Zeiss Crossbeam 540 Scanning Electron Microscope, to prevent damaging the polymer or CNTs by the ion beam. H-shaped lamellae were obtained by milling normally to the composite cross sections (parallel to the CNT alignment direction). Microtome sectioning was also used to prepare 60-nm thick TEM lamellae by cutting normal to the CNT alignment direction. Prior to microtoming, small sections (~1.5 mm) of the CNT-PMPI composites were embedded in EMbed 812 according to a multi-step procedure. First, the specimens were placed in a vial and immersed in 200 proof EM grade ethanol overnight, followed by soaking in a 50:50 mixture of ethanol and embedding resin for two days. In both of those stages, the vial was kept in a tube rotator to ensure agitation of the liquid medium. Second, the soaked samples were laid out in a flat silicone embedding mold, covered by a thin layer of resin, and cured at 60°C for one day. After curing, the samples were flipped over in the embedding mold and a layer of fresh resin was poured on top, followed by curing in the same conditions. This two-step embedding process ensures centering of the CNT composite within the resin. Microtoming was performed with a histology diamond knife at room temperature on a Leica Ultracut UCT. TEM was performed on both a high resolution JEOL 2100F TEM and a Hitachi 7800 TEM.

Thermogravimetric analysis: Thermogravimetric analysis (TGA) was performed on a TA instrument Discovery TGA. The sample was cut in small pieces and a mass of approximately 1 mg was put into a Platinum HT pan. The temperature was ramped up from 40°C to 900°C at a heating rate of 10°C min^{-1} in Nitrogen. The TGA data was then analyzed using TA instrument software TRIOS to find the onset temperature and polymer content. For the different monomer concentrations and solvents, we calculated the polymer content and onset temperature in accordance with ASTM® E2550 – 17 standard. Three samples synthesized in the same conditions were tested by TGA to obtain the standard deviation on the onset temperature and polymer content.

Uniaxial tensile testing: The CNT ribbons were cut with a stainless steel scalpel into dog-bone specimens following ISO- 37 standard (Type 4 geometry) prior to being tested. The cut was performed using an acrylic mask which featured a path where the scalpel could be inserted to cut the CNT ribbon pressed between the acrylic mask and a cutting mat. Uniaxial tensile testing was performed at a strain rate of 3mm min^{-1} on an Instron 8848 MicroTester equipped with a 50 N load cell. Five to seven samples synthesized in the same conditions were mechanically tested to obtain values of elastic modulus and tensile strength as well as the standard deviation.

X-ray tomography: X-ray tomography was performed on a Zeiss Versa 520 machine, adjusting the source and detector distances to obtain a voxel size of 2 µm. The sample was clamped with the long axis of the ribbon pointing in the vertical direction. Rotation axis corresponded to the long axis of the ribbon (alignment direction of the CNTs). Data acquisition was controlled with the software Scout-and-Scan™ Control System. A 3D image was generated from the individual slices using the software Dragonfly 4.1.

Supporting Information

Supporting Information is available from the Wiley Online Library or from the author.

Acknowledgements

Financial support was provided by the NASA Space Technology Research Institute (STRI) for Ultra-Strong Composites by Computational Design (US-COMP, grant NNX17AJ32G). C.K.J. also acknowledges funding from the MIT Undergraduate Research Opportunities (UROP) Program. We thank Claire Jolowski and Prof. Zhiyong (Richard) Liang of Florida State University, as well as Nanocomp Technologies (a subsidiary of Huntsman Advanced Materials), for providing the CNT sheets. We thank the Koch Institute's Peterson (1957) Nanotechnology Materials Core Facility for technical support, specifically David Mankus for assistance with Cryo-FIB and Dong Soo Yun for performing high-resolution TEM imaging. We also thank the Harvard Center for Nanoscale Systems, particularly Nicki Watson for assistance with microtome sectioning and TEM imaging. We thank Reed Kopp (MIT), for assistance with X-ray CT measurements. We also thank William. J. Sawyer, Ashley L. Kaiser, Megan Creighton, Joseph D. Sandt, Richard B. Church, and Nick T. Dee of MIT, and Dr. Mathias C. Celina from Sandia National Laboratories, for useful discussions regarding this work. C.A.C.C. and A.J.H. are inventors on patent application US16/663,313 Systems, devices, and methods for promoting *in-situ* polymerization within nanomaterial assemblies.

References

[1] J. N. Coleman, U. Khan, W. J. Blau, Y. K. Gun'ko, *Carbon N. Y.* **2006**, *44*, 1624.

[2] Y.-Y. Fan, A. Kaufmann, A. Mukasyan, A. Varma, *Carbon N. Y.* **2006**, *44*, 2160.

[3] J.-M. Feng, R. Wang, Y.-L. Li, X.-H. Zhong, L. Cui, Q.-J. Guo, F. Hou, *Carbon N. Y.* **2010**, *48*, 3817.

[4] L. Weller, F. R. Smail, J. A. Elliott, A. H. Windle, A. M. Boies, S. Hochgreb, *Carbon N. Y.* **2019**, *146*, 789.

[5] C. A. C. Chazot, A. J. Hart, *Compos. Sci. Technol.* **2019**, *183*, 107795.

[6] J. Zhu, W. Cao, M. Yue, Y. Hou, J. Han, M. Yang, *ACS Nano* **2015**, *9*, 2489.

[7] K. K. K. Koziol, S. Boncel, M. S. P. Shaffer, A. H. Windle, *Compos. Sci. Technol.* **2011**, *71*, 1606.

[8] W. Guo, C. Liu, X. Sun, Z. Yang, H. G. Kia, H. Peng, *J. Mater. Chem.* **2012**, *22*, 903.

[9] S. Zhang, L. Zhu, C. P. Wong, S. Kumar, *Macromol. Rapid Commun.* **2009**, *30*, 1936.

[10] W. Zhao, Y. Li, S. Wu, D. Wang, X. Zhao, F. Xu, M. Zou, H. Zhang, X. He, A. Cao, *ACS Appl. Mater. Interfaces* **2016**, *8*, 34027.

[11] H. Zhang, G. Cao, Z. Wang, Y. Yang, Z. Shi, Z. Gu, *Electrochem. commun.* **2008**, *10*, 1056.

[12] W. Feng, X. D. Bai, Y. Q. Lian, J. Liang, X. G. Wang, K. Yoshino, *Carbon N. Y.* **2003**, *41*, 1551.

[13] S. Kim, F. Fornasiero, H. G. Park, J. Bin In, E. Meshot, G. Giraldo, M. Stadermann, M. Fireman, J. Shan, C. P. Grigoropoulos, O. Bakajin, *J. Memb. Sci.* **2014**, *460*, 91.

[14] P. C. Hiemenz, T. P. Lodge, *Polymer Chemistry - Second Edition*; 2007.

[15] P. W. Morgan, In *Encyclopedia of Polymer Science and Technology*; John Wiley & Sons, Inc., 2011.

[16] E. E. Magat, Formation of Films And Filament Directly from Polymer Intermediates **1955**.

[17] R. E. Whitfield, L. A. Miller, W. L. Wasley, *Text. Res. J.* **1961**, *31*, 704.

[18] J. M. Gohil, P. Ray, *Sep. Purif. Technol.* **2017**, *181*, 159.

[19] J.-Y. Jeong, H.-J. Lee, S.-W. Kang, L.-S. Tan, J.-B. Baek, *J. Polym. Sci. Part A Polym. Chem.* **2008**, *46*, 6041.

[20] R. Haggenmueller, F. Du, J. E. Fischer, K. I. Winey, *Polymer (Guildf).* **2006**, *47*, 2381.

[21] M. Moniruzzaman, J. Chattopadhyay, W. E. Billups, K. I. Winey, *Nano Lett.* **2007**, *7*, 1178.

[22] C. Jolowsky, R. Sweat, J. G. Park, A. Hao, R. Liang, *Compos. Sci. Technol.* **2018**, *166*, 125.

[23] M. D. Yadav, K. Dasgupta, A. W. Patwardhan, J. B. Joshi, *Ind. Eng. Chem. Res.* **2017**, *56*, 12407.

[24] Chloroform - International Labour Organization card **2000**.

[25] Cyclohexanone - International Labour Organization card **2004**.

[26] J. H. Saunders, F. Dobinson, In *Non Radical Polymerization*; Bamford, C. H.; Tipper, C. F. H., Eds.; NEW YORK, 1976.

[27] A. V. Berezkin, R. Khokhlov, Alexei, *J. Polym. Sci. Part B Polym. Phys.* **2006**, *44*, 2698.

[28] R. J. Zdrahala, E. M. Firer, J. F. Fellers, *J Polym Sci Polym Chem Ed* **1977**, *15*, 689.

[29] P. W. Morgan, S. L. Kwolek, *J. Polym. Sci.* **1959**, *40*, 299.

[30] R. Malik, C. McConnell, N. T. Alvarez, M. Haase, S. Gbordzoe, V. Shanov, *RSC Adv.* **2016**, *6*, 108840.

[31] F. Fang, S. P. Lake, *Interface Focus* **2016**, *6*.

[32] A. L. Butcher, C. T. Koh, M. L. Oyen, *J. Mech. Behav. Biomed. Mater.* **2017**, *69*, 412.

[33] Y. Bai, R. Zhang, X. Ye, Z. Zhu, H. Xie, B. Shen, D. Cai, B. Liu, C. Zhang, Z. Jia, S. Zhang, X. Li, F. Wei, *Nat. Nanotechnol.* **2018**, *13*, 589.

[34] H. I. Kim, M. Wang, S. K. Lee, J. Kang, J. Do Nam, L. Ci, J. Suhr, *Sci. Rep.* **2017**, *7*.

[35] D. A. Hernandez, C. A. Soufen, M. O. Orlandi, *Mater. Res.* **2017**, *20*, 951.

[36] G. T. Truong, J. Kim, K. K. Choi, *Adv. Mater. Sci. Eng.* **2018**.

[37] G. Hou, R. Su, A. Wang, V. Ng, W. Li, Y. Song, L. Zhang, M. Sundaram, V. Shanov, D. Mast, D. Lashmore, M. Schulz, Y. Liu, *Carbon N. Y.* **2016**, *102*, 513.

[38] K. G. Dassios, *Mater. Sci. Appl.* **2012**, *03*, 658.

[39] W. Ding, A. Eitan, F. T. Fisher, X. Chen, D. A. Dikin, R. Andrews, L. C. Brinson, L. S. Schadler, R. S. Ruoff, *Nano Lett.* **2003**, *3*, 1593.

[40] A. Kumano, H. Oguro, T. Hayashi, COMPOSITE HOLLOW FIBER MEMBRANE AND PROCESS FOR ITS PRODUCTION **1998**.

[41] M. N. A. Seman, M. Khayet, N. Hilal, *J. Memb. Sci.* **2010**, *348*, 109.

[42] H. Ichiura, K. ichi Yamamoto, Y. Ohtani, *Polym. Bull.* **2015**, *72*, 2621.

[43] S. Yang, H. Zhen, B. Su, *RSC Adv.* **2017**, *7*, 42800.

[44] L. Thi Mai Hoa, *Diam. Relat. Mater.* **2018**, *89*, 43.

Keywords

carbon nanotubes, polymerization, interface, composites, mechanics

Title

In-Situ Interfacial Polymerization: A Technique for Rapid Formation of Highly Loaded Carbon Nanotube-Polymer Composites.

Cécile A. C. Chazot, Carolyn K. Jons, and A. John Hart*

TOC figure